Nanoscale separation of molecular species based on their rotational mobility

Ilaria Testa, Andreas Schönle*, Claas v. Middendorff, Claudia Geisler, Rebecca Medda, Christian A. Wurm, Andre C. Stiel, Stefan Jakobs, Mariano Bossi, Christian Eggeling, Stefan W. Hell, and Alexander Egner

Department of NanoBiophotonics, Max-Planck-Institute for Biophysical Chemistry, Am Fassberg 11, 37077 Göttingen, Germany
**Corresponding author: aschoen@gwdg.de*

Abstract: We combine far-field fluorescence nanoscopy through serialized recording of switchable emitters with polarization-sensitive fluorescence detection. In addition to imaging with nanoscale spatial resolution, this technique allows determination of the fluorescence anisotropy of each detected dipole emitter and thus an estimate of its rotational mobility. Sub-populations of fluorescent markers can thus be separated based on their interaction with the sample. We applied this new functional nanoscopy to imaging of living mammalian cells.

OCIS codes: (110.0180) Imaging systems: Microscopy; (170.3880) Medical optics and biotechnology : Medical and biological imaging; (170.6280) Medical optics and biotechnology : Spectroscopy, fluorescence and luminescence; (180.2520) Microscopy : Fluorescence microscopy

References and links

1. E. Abbe, "Beiträge zur Theorie des Mikroskops und der mikroskopischen Wahrnehmung," Arch. Mikr. Anat. **9**, 413-468 (1873).
2. S. W. Hell, "Improvement of lateral resolution in far-field light microscopy using two-photon excitation with offset beams," Opt. Commun. **106**, 19-24 (1994).
3. S. W. Hell and J. Wichmann, "Breaking the diffraction resolution limit by stimulated emission: stimulated emission depletion microscopy," Opt. Lett. **19**, 780-782 (1994).
4. S. W. Hell, "Toward fluorescence nanoscopy," Nature Biotechnol. **21**, 1347-1355 (2003).
5. S. W. Hell, "Far-Field Optical Nanoscopy," Science **316**, 1153-1158 (2007).
6. T. A. Klar, S. Jakobs, M. Dyba, A. Egner, and S. W. Hell, "Fluorescence microscopy with diffraction resolution limit broken by stimulated emission," Proc. Nat. Acad. Sci. U.S.A **97**, 8206-8210 (2000).
7. E. Betzig, G. H. Patterson, R. Sougrat, O. W. Lindwasser, S. Olenych, J. S. Bonifacino, M. W. Davidson, J. Lippincott-Schwartz, and H. F. Hess, "Imaging Intracellular Fluorescent Proteins at Nanometer Resolution," Science **313**, 1642-1645 (2006).
8. M. J. Rust, M. Bates, and X. Zhuang, "Sub-diffraction-limit imaging by stochastic optical reconstruction microscopy (STORM)," Nat. Methods **3**, 793-796 (2006).
9. S. T. Hess, T. P. K. Girirajan, and M. D. Mason, "Ultra-High Resolution Imaging by Fluorescence Photoactivation Localization Microscopy," Biophys. J. **91**, 4258-4272 (2006).
10. A. Egner, C. Geisler, C. von Middendorff, H. Bock, D. Wenzel, R. Medda, M. Andresen, A.-C. Stiel, S. Jakobs, C. Eggeling, A. Schönle, and S. W. Hell, "Fluorescence nanoscopy in whole cells by asnychronous localization of photoswitching emitters," Biophys. J. **93**, 3285-3290 (2007).
11. W. Heisenberg, *The physical principles of the quantum theory* (Chicago Univ Press, Chicago, 1930).
12. N. Bobroff, "Position measurement with a resolution and noise-limited instrument," Rev. Sci. Instrum. **57**, 1152-1157 (1986).
13. E. Betzig, "Proposed method for molecular optical imaging," Opt. Lett. **20**, 237-239 (1995).
14. S. W. Hell, J. Soukka, and P. E. Hänninen, "Two- and multiphoton detection as an imaging mode and means of increasing the resolution in far-field light microscopy," Bioimaging **3**, 65-69 (1995).
15. T. Schmidt, G. J. Schutz, W. Baumgartner, H. J. Gruber, and H. Schindler, "Imaging of single molecule diffusion," Proc. Natl. Acad. Sci. USA **93**, 2926-9 (1996).
16. T. D. Lacoste, X. Michalet, F. Pinaud, D. S. Chemla, A. P. Alivisatos, and S. Weiss, "Ultrahigh-resolution multicolor colocalization of single fluorescent probes," Proc. Natl. Acad. Sci. USA **97**, 9461-9466 (2000).
17. R. E. Thompson, D. R. Larson, and W. W. Webb, "Precise nanometer localization analysis for individual fluorescent probes," Biophys. J. **82**, 2775-2783 (2002).
18. W. E. Moerner and L. Kador, "Optical detection and spectroscopy of single molecules in a solid," Phys. Rev. Lett. **62**, 2535-2538 (1989).

#104042 - $15.00 USD Received 12 Nov 2008; revised 3 Dec 2008; accepted 3 Dec 2008; published 4 Dec 2008

19. M. Orrit and J. Bernard, "Single pentacene molecules detected by fluorescence excitation in a p-terphenyl crystal," Phys. Rev. Lett. **65**, 2716-2719 (1990).
20. E. B. Shera, N. K. Seitzinger, L. M. Davis, R. A. Keller, and S. A. Soper, "Detection of single fluorescent molecules," Chem. Phys. Lett. **174**, 553-557 (1990).
21. T. Ha, T. Enderle, D. F. Ogletree, D. S. Chemla, P. R. Selvin, and S. Weiss, "Probing the interaction between two single molecules: Fluorescence resonance energy transfer between a single donor and a single acceptor," Proc. Natl. Acad. Sci. USA **93**, 6264-6268 (1996).
22. A. Schönle and S. W. Hell "Fluorescence nanoscopy goes multicolor," Nature Biotechnol. **25**, 1234-1235 (2007).
23. M. Bossi, J. Fölling, V. N. Belov, V. P. Boyarskiy, R. Medda, A. Egner, C. Eggeling, A. Schönle, and S. W. Hell, "Multi-color far-field fluorescence nanoscopy through isolated detection of distinct molecular species," Nano Lett. **8**, 2463-2468 (2008).
24. M. Andresen, A. C. Stiel, J. Fölling, D. Wenzel, A. Schönle, A. Egner, C. Eggeling, S. W. Hell , and S. Jakobs, "Photoswitchable fluorescent proteins enable monochromatic multilabel imaging and dual color fluorescence nanoscopy," Nat. Biotechnol. **26**, 1035 - 1040 (2008).
25. T. Ha, T. Enderle, D. S. Chemla, P. R. Selvin, and S. Weiss, "Single molecule dynamics studied by polarization modulation," Phys. Rev. Lett. **77**, 3979-3982 (1996).
26. J. Schaffer, A. Volkmer, C. Eggeling, V. Subramaniam, G. Striker, and C. A. M. Seidel, "Identification of single molecules in aqueous solution by time-resolved fluorescence anisotropy," J. Phys. Chem. A **103**, 331-336 (1999).
27. J. Fölling, V. Belov, R. Kunetsky, R. Medda, A. Schönle, A. Egner, C. Eggeling, M. Bossi, and S. W. Hell, "Photochromic Rhodamines Provide Nanoscopy with Optical Sectioning," Angew. Chem. Int. Ed. **46**, 6266-6270 (2007).
28. A. van Blaaderen and A. Vrij, "Synthesis and Characterization of Colloidal Dispersions of Fluorescent, Monodisperse Silica Spheres," Langmuir **8**, 2921-2931 (1992).
29. J. Fölling, V. Belov, D. Riedel, A. Schönle, A. Egner, C. Eggeling, M. Bossi, and S. W. Hell "Fluorescence Nanoscopy with Optical Sectioning by Two-Photon Induced Molecular Switching using Continuous-Wave Lasers," ChemPhysChem **9**, 321 - 326 (2008).
30. A. C. Stiel, M. Andresen, H. Bock, M. Hilbert, J. Schilde, A. Schönle, C. Eggeling, A. Egner, S. W. Hell, and S. Jakobs, "Generation of Monomeric Reversibly Switchable Red Fluorescent Proteins for Far-Field Fluorescence Nanoscopy," Biophys. J. **95**, 2989–2997 (2008).
31. J. Wiedenmann, S. Ivanchenko, F. Oswald, F. Schmitt, C. Röcker, A. Salih, K.-D. Spindler, and G. U. Nienhaus, "EosFP, a fluorescent marker protein with UV-inducible green-to-red fluorescence conversion," Proc.Natl.Acad.Sci.USA **101**, 15905-15910 (2004).
32. P. Lamesch, N. Li, S. Milstein, C. Fan, T. Hao, G. Szabo, Z. Hu, K. Venkatesan, G. Bethel, P. Martin, J. Rogers, S. Lawlor, S. McLaren, A. Dricot, H. Borick, M. E. Cusick, J. Vandenhaute, I. Dunham, D. E. Hill, and M. Vidal, "hORFeome v3.1: A resource of human open reading frames representing over 10,000 human genes," Genomics **89**, 307-315 (2007).
33. C. Geisler, A. Schönle, C. von Middendorff, H. Bock, C. Eggeling, A. Egner, and S. W. Hell "Resolution of λ/10 in fluorescence microscopy using fast single molecule photo-switching," Appl. Phys. A **88**, 223-226 (2007).
34. J. Enderlein, "Theoretical study of detection of a dipole emitter through an objectiv with high numerical aperture," Opt. Lett. **25**, 634-636 (2000).
35. K. Bacia and P. Schwille, "A dynamic view of cellular processes by in vivo fluorescence auto- and cross-correlation spectroscopy," Methods **29**, 74-85 (2003).
36. T. L. Hill and M. W. Kischner, "Subunit treadmilling of microtubules or actin in the presence of cellular barriers: possible conversion of chemical free energy into mechanical work," Proc. Natl. Acad. Sci. USA **79**, 490-494 (1982).
37. C. Zander, M. Sauer, K. H. Drexhage, D.-S. Ko, A. Schulz, J. Wolfrum, L. Brand, C. Eggeling, and C. A. M. Seidel, "Detection and characterization of single molecules in aqueous solution," Appl. Phys. B **63**, 517-523 (1996).
38. J. Fölling, M. Bossi, H. Bock, R. Medda, C. A. Wurm, B. Hein, S. Jakobs, C. Eggeling, and S. W. Hell "Fluorescence nanoscopy by ground-state depletion and single-molecule return," Nat. Meth. **5**, 943 - 945 (2008).

1. Introduction

Fluorescence far-field optical microscopy is one of the most important tools in life science. Highly specific tagging with fluorescent markers allows functional imaging of intact and even living samples using visible light with minimal impact on the system under consideration. By tagging different molecular species with different types of markers, their spatial and temporal correlation can be explored. Importantly, the markers themselves can function as ultra-small chemical or physical sensors reporting on their micro-environment by changing their spectroscopic properties. Depending on for example, pH, temperature or binding state, the

#104042 - $15.00 USD Received 12 Nov 2008; revised 3 Dec 2008; accepted 3 Dec 2008; published 4 Dec 2008

markers' emission can be used to classify their immediate vicinity. One has long argued that a severe drawback of using far-field optical microscopy is its limited resolution which impedes the separation of similar objects which are closer together than about half of the wavelength used (~250nm). The resolution limit also hampers the detection of the spectroscopic properties of the marker in bulk measurements because unlike in single molecule spectroscopy of dilute solutions, fluorescence is simultaneously detected for several of the densely packed labels. The physical reason for this fundamental limit [1] is diffraction, which leads to an irrecoverable loss of information as the light travels from the emitter to the imaging lens.

In the early 1990's it was discovered that the diffraction barrier in far-field optical microscopy can be fundamentally overcome by exploiting selected transitions between the states of the marker [2,3]. Specifically, the marker can be switched between a fluorescent "on" and a non-fluorescent "off" state, which can then be used to confine the origin of the fluorescence emission in space and therefore to read out additional spatial information sequentially from sub-diffraction sized regions [4,5]. While early implementations of this concept such as stimulated emission depletion (STED) microscopy were based on deterministic scanning of a squeezed detection volume over the sample [3,6], the introduction of meta-stable optically switchable markers into superresolution imaging [4] has triggered the development of stochastic readout schemes: at any given point in time, very few individual markers are randomly switched to their fluorescent state and detected one after other [7-10]. In doing so, it is mandatory that the labels in the on-state are well-isolated and each of them emits a large number of photons in a stream in order to determine its position with high precision [11-17].

However, position is only one aspect of the information encoded into the label's photon stream. Wavelength, detection time and polarization also carry additional information. While previously many labels were detected together resulting in the measurements of mean values of these parameters, they can now be recorded on a single emitter basis [18-21]. A plethora of methods known from single-molecule spectroscopy can now be used for analysis in fluorescence nanoscopy [22]. For example, the detection of two spectral channels acquires enough information to separate three or more molecular species with the maxima of their emission spectra separated less than 30nm [23,24]. An other logical choice is to measure the polarization state of the photon stream to infer fluorescence anisotropy and thus mobility or orientation of each single emitter [25,26].

Here, we show that switching of single isolated emitters in combination with detection of different polarization directions allows recording of fluorescence images with nanoscale resolution and simultaneously to distinguish between molecular species of different mobility. We depict how the creation of anisotropy histograms yields information about rotational diffusion in the millisecond time range, which is normally not accessible through conventional fluorescence anisotropy measurements. Images of the endoplasmic reticulum and of the actin network of live mammalian cells, labeled with photoswitchable fluorescent proteins, depict a mobility map with nanoscale resolution and exemplify the power of this functional nanoscopy approach.

2. Materials and methods

2.1 Sample preparation

For the experiments verifying the theoretical findings and exemplifying the discrimination between molecular species of different mobility, several samples containing a photoactivatable variant of Rhodamine B (pcRhB) [27] were prepared. (i) pcRhB fixed in a poly methyl methacrylate (PMMA) film was prepared by spin coating of a solution of pcRhB (1µM) in PMMA (4mg/ml) on a microscope coverslip and drying of the sample for over 24 hours. (ii) pcRhB mounted in mowiol was prepared by spin coating a solution of pcRhB (1µM) in mowiol on a microscope coverslip directly before the experiment. (iii) A mixture of ~ 75nm large pcRhB labeled core-shell particles and of pcRhB in mowiol was prepared by

#104042 - $15.00 USD Received 12 Nov 2008; revised 3 Dec 2008; accepted 3 Dec 2008; published 4 Dec 2008

initially evaporating a suspension of pcRhB labeled beads in ethanol onto a microscope coverslip. Thereafter, the sample was mounted with the pcRhB / mowiol solution as already mentioned in (ii). The pcRhB labeled small core–shell silica particles were prepared as described previously [28,29]. Briefly, the photochromic dye was incorporated into ~74 nm diameter spheres and a pure silica shell of 22nm thickness was then afterwards grown onto these cores. All sizes were determined by transmission electron microscopy (TEM).

For the measurements of living PtK2 cells we prepared basically two different kinds of samples. (i) The reversible photoswitchable fluorescent protein rsCherryRev was targeted to the lumen of the endoplasmic reticulum (ER) as described previously [30]. (ii) The β-actin (Actb) was fused to the photoswitchable fluorescent protein tdEosFP [31]. The tdEosFP-plasmid was constructed using standard cloning methods: To tag Actb at its C-terminus with tdEosFP, the expression plasmid pH-ActB-tdEosFP was constructed by Gateway vector conversion (Invitrogen, Carlsbad, CA, USA) from the donor vector pDONR223-Actb [32] and the empty destination vector pMD-tdEosFP-N.

For transfection, cells were grown overnight, as described previously [30], on glass cover slips to ~ 80% confluence. The plasmids were introduced using the Nanofectin kit according to the manufacturer's instructions (PAA, Pasching, Austria). Briefly, 3µg DNA were used for one well of a six well plate. One day after the transfection, cells expressing the fluorescent proteins became visible. Typically they were imaged within the following day. For imaging the cell, culture medium was replaced by HDMEM (10mM HEPES buffered Dulbecco's Modified Eagle Medium DMEM without phenolred).

For the depolymerization of filamentous actin (F-actin), we added two days after transfection, 40µg/ml of the toxin latrunculin B directly to the culture medium of the β-actin-tdEosFP transfected cells and incubated for 15 to 25 minutes under standard growth conditions. For the recovery of the F-actin, we replaced the toxin containing medium with normal culture medium and incubated for another 30 minutes under normal conditions.

2.2 Microscopy setup and single molecule nanoscopy

A scheme of our nanoscopy setup is shown in Fig. 1. We either used a 532nm laser diode pumped solid state laser (Shanghai Laser Century Technology Co., Shanghai, China) or a 560nm fiber laser (MPB Communications, Montreal, Canada) for fluorescence excitation and a 405nm diode laser (Coherent, CA, USA) for photoswitching. The laser beams were combined by a dichroic filter (Z 415 RDC, AHF Analysentechnik, Tübingen, Germany) and subsequently coupled into a regular commercial wide-field microscope (DMIRE 2, Leica Microsystems, Wetzlar, Germany) using several mirrors. The laser power was controlled by an acousto-optical tunable filter (Pegasus Optics GmbH, Wallenhorst, Germany). Uniform epi-illumination of a field of view of ~10µm in diameter was achieved by under-illuminating the back aperture of the objective lens (HCX APO 100x/1.30 Oil U-V-I 0.17/D, Leica Microsystems). A quarter wave plate (375/550nm, B.Halle Nachfl. GmbH, Berlin, Germany) was inserted into the illumination path to ensure nearly circular polarization of all laser light. The fluorescence emitted by the sample was collected by the same objective lens, separated from the laser light by a dichroic filter (Z532/NIRrpc for the pcRhB molecules and Z580dcxr for the photoswitchable proteins; AHF Analysentechnik) and subsequently split by a broad band polarizing beam splitter cube (OptoSigma, Santa Ana, CA, USA). The two beams of different polarization states were then imaged onto different areas of the electron multiplying CCD camera's chip (IXON-Plus DU-860, Andor Technology, Belfast, Northern Ireland). One pixel on the camera corresponded to an area of $96x96nm^2$ in the image plane. Residual laser light was removed by a notch filter (NF01-532U-25 for the experiments with pcRhB and NF01-568U-25 (tilted) for the experiments with rsCherryRev and tdEosFP, AHF Analysentechnik) and the detection range was limited to the labels' respective emission spectrum by a bandpass filter (for pcRhB: FF01-582/75-25, for rsCherryRev: ET630/75M, and for tdEosFP: HQ610/75, AHF Analysentechnik).

#104042 - $15.00 USD Received 12 Nov 2008; revised 3 Dec 2008; accepted 3 Dec 2008; published 4 Dec 2008

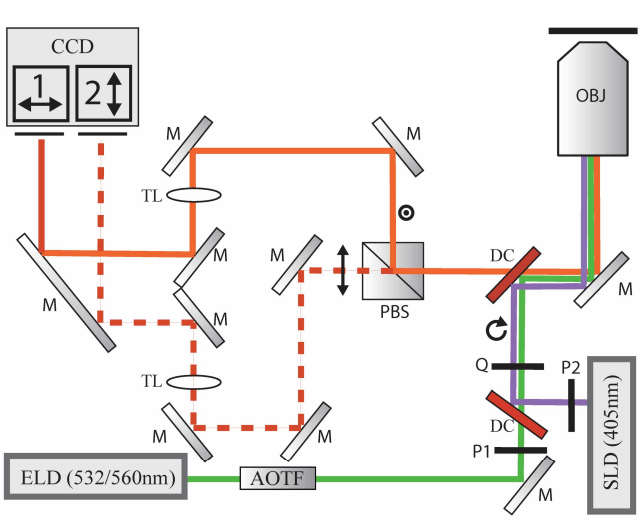

Fig. 1. The microscope setup is essentially a regular wide-field microscope equipped with a fast and sensitive CCD camera for detection of single emitters and a choice of several laser sources and beam optics for switching and excitation with circularly polarized light. Fluorescence is split into the two polarization channels by a polarizing beam splitter (PBS) and imaged onto separate areas (1,2) of the same CCD chip. A more detailed description is given in the text. Labels: (ELD) excitation laser diode, (SLD) switching laser diode, (AOTF) acousto-optical tunable filter, (M) mirror, (P1, P2) polarizer, (DC) dichroic filter, (Q) quarter wave plate, (OBJ) objective lens, (PBS) polarizing beamsplitter, (TL) tube lens and (CCD) EMCCD camera.

We used the photo-switchability of the fluorescent labels to create sub-diffraction resolution images in the following way [7-10]: the labels were normally in a dark off-state (for tdEosFP, we refer to its green fluorescent state as the off-state) and transferred into their on-state by irradiation with 405nm light. A low intensity of the 405nm switch-on light ensured that a low enough fraction of labels were in their on-state at a given time (or, more precisely, at any time during one camera frame recording) to ensure imaging of single isolated molecules, e.g. < 1 fluorescent molecule per diffraction-limited area of ~280nm diameter. After emitting a stream of photons, a bright molecule goes back into a dark off-state, e.g. by photobleaching or switching to a non-fluorescent state due to the excitation light. Subsequent switching-on of other isolated molecules allowed the recording of the next fluorescence spots. From the recorded fluorescence, the positions of the individual molecules could be determined with a precision superior to the diffraction-limited resolution, as outlined in the next paragraph. We used an asynchronous acquisition mode previously termed PALMIRA [10,33] where the image acquisition was run continuously until a large enough number of molecular positions could be determined to generate the final high-resolution image.

The initial localization of single switching events was performed independently on both channels and followed the same procedure as described earlier [33]: In a first step, possible non-uniform background from out-of-focus fluorescence was removed by smoothing the image with a Gaussian of full width at half maximum (FWHM) of about three times the microscope's resolution and subtracting this result from the raw data. A segmentation algorithm then identified regions of at least three connected pixels exhibiting more than 105 counts. A fix-point iteration [17] was hereafter used to determine the center position of these spots. Depending on their location on the CCD chip, the localized spots were assigned to either one of the two detection channels. Calibration measurements were regularly performed on fluorescent beads emitting into both channels and the affine transformation between the two channels was determined that resulted in the best co-localization. This transformation was later on used to match the points belonging to the very same event. For unmatched points, indicating events where the signal in one of the channels was below threshold, this

#104042 - $15.00 USD Received 12 Nov 2008; revised 3 Dec 2008; accepted 3 Dec 2008; published 4 Dec 2008

transformation was also used to determine the starting point for an additional run of the fix-point iteration. The final position of an event was then determined as the photon number weighted mean of the positions determined independently in the two channels. Event brightness was calculated from the Gaussian weighted sum of each fluorescent spot. We chose the width of the Gaussian to match that of the fluorescent spots resulting in a correction factor of two. We also corrected for the camera gain factor of 7.5 and a slight difference in the detection efficiency between the two channels (ch1/ch2 = 1.1 and 1.2 for the pcRhB and protein set-up configuration, respectively). The position of each event and the number of detected photons in both channels was then recorded in a data file for further use.

3. Theory

The goal in our polarization dependent nanoscale imaging approach is to separate molecular species due to their rotational mobility. To this end, we have to know how each detected event can be assigned to one of the species present in the sample. In bulk measurements, a detected event is a single photon and the only way to identify it with a species is directly by the channel in which it was detected. In our case, a detected event is a stream of photons of which n_1 are detected in the first and n_2 are detected in the second channel, each monitoring different directions of polarization. Hence there will be a characteristic distribution of probable count pairs (n_1, n_2) for each species, which can be used for species identification.

We describe the orientation of an emitter in the sample by the azimuthal angle θ its emission dipole forms with the optical axis and by the polar angle ϕ it forms with the in plane x-axis, e.g. the polarization direction of channel 1. We further define $f(n)$ as the probability that n photons are emitted by a switched-on marker during any given camera frame. This probability distribution will strongly depend on experimental details, including the excitation intensity and the photobleaching yield of the fluorophores. Usually $f(n)$ is well approximated by a geometrical distribution $f(n;N)$ with an average N. Only if the frame integration time is too low, i.e., if it is shorter than the average on-time of a fluorophore, the distribution of photon numbers will change to a Poissonian and an additional dependence on the exposure time and the excitation and emission rate of the fluorophore has to be introduced. As the fluorescence is split into the two polarization channels, we denote the conditional probability that a detected photon is registered in either of the two channels as $p_i(\theta,\phi)$, which for example can be calculated using the vectorial collection efficiency of the microscope [34]. The sensitive timescale in our experiments is defined by the duration T of the fluorescence burst from an emitter after switching it to its on-state. If the emitter rotates much faster than T, the probability of detecting a photon in each of the channels is equal due to symmetry. The probability of detecting n_1 photons in channel 1 and n_2 photons in channel 2 is therefore given by

$$g(n_1,n_2) = f(n_1+n_2; N\,p)2^{-n_2-n_1}(n_1+n_2)!/(n_1!n_2!) \qquad (1)$$

where p denotes the total probability of detecting an emitted photon in either one of the channels. Here we used the fact that the convolution of a geometric distribution and binomial probability distribution is again geometric.

If, on the other hand, the emitter rotates much slower than T, this averaging does not occur. If we take into account that we use circularly polarized light for switching and excitation (Fig. 1) and if we also assume that the number of emitted photons is independent of the markers orientation, which is an acceptable approximation if the camera frame times are longer than the burst time T, we have

$$g(n_1,n_2) = \int d\Omega\, f(n_1,n_2; N\,p(\theta))\, p_1(\theta,\phi)^{n_1}\, p_2(\theta,\phi)^{n_2}(n_1+n_2)!/(n_1!n_2!) \qquad (2)$$

for the static case. Here $p(\theta)$ is the overall probability of detecting a photon emitted from a marker forming an angle θ with the optic axis. In this initial study, we do not aim at a quantitative analysis of rotational diffusion times, but rather at separating molecular species

#104042 - $15.00 USD Received 12 Nov 2008; revised 3 Dec 2008; accepted 3 Dec 2008; published 4 Dec 2008

based on strong differences in their mobility. Therefore we neglect the effect of depolarization due to the high-angle focusing [34] and use $p_1(\theta,\phi) = \cos^2(\phi)$, $p_2(\theta,\phi) = \sin^2(\phi)$ and $p(\theta) = 3p\sin^2(\theta)/2$ as a rough approximation for the orientation-dependent collection efficiency of the optical system.

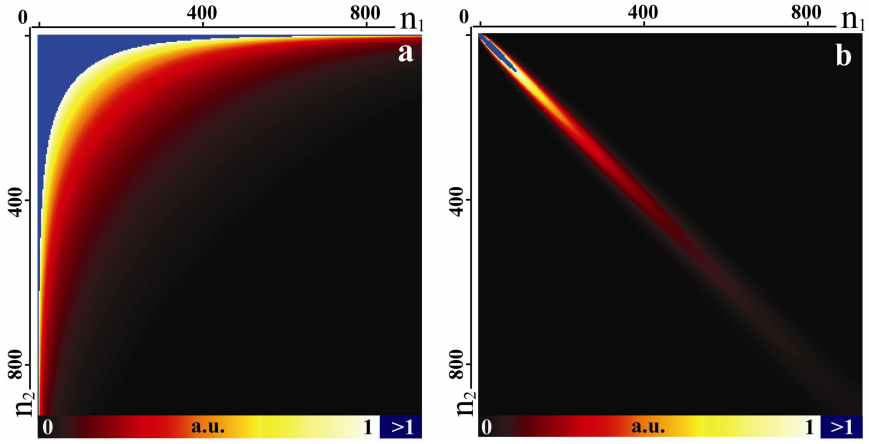

Fig. 2. Theoretical two-dimensional anisotropy histogram for (a) fixed molecules and (b) molecules rotating much faster than the typical single molecule fluorescence burst duration calculated as predicted by equations (1) and (2). Depolarization due to focusing through a large aperture lens, detection background and slower rotation speeds were not considered and will lead to broader distributions in experimental histograms.

Experimentally we can measure $g(n_1, n_2)$ by plotting a two-dimensional frequency histogram of the photon pairs (n_1, n_2) detected from a multitude of single isolated molecules. We will refer to these plots as two-dimensional anisotropy histograms throughout this paper. Theoretical predictions of the two-dimensional anisotropy histograms for static and the fast rotating molecular species are depicted in Fig. 2. We used $\mathcal{N}p=680$ as the average number of detected photons, as this number is close to our experimental observations. Obviously, the two distributions differ strongly. For static markers, all photons emitted during a single event are polarized along the marker's direction and as $p_1(\theta,\phi) = \cos^2(\phi)$ and $p_2(\theta,\phi) = \sin^2(\phi)$ we expect an uneven distribution of the photons in the two channels. This is reflected in the histogram (Fig. 2(a)) which mainly extends along the two axes n_1 and n_2. Fast rotating molecules on the other hand, distribute their photons evenly into both polarization directions and thus their events are located along the bisecting axis of the histogram (Fig. 2(b)). Molecular species with rotational diffusion times in the order of the burst time T or with partial mobility will naturally produce intermediate distributions. We also define the fluorescence polarization of individual single molecule events

$$P_n = (n_2 - n_1)/(n_1 + n_2). \tag{3}$$

as a measure for further classification.

4. Experimental results

As an initial experiment to verify our theoretical predictions, we prepared two samples of the photochromic dye pcRhB: one in PMMA where the dye molecules are fixed and one in mowiol where they still have rotational freedom. In thermal equilibrium and at neutral pH, pcRhB is predominantly in its dark state but can be transferred to its on-state by irradiation with UV light [27]. Switching-off of pcRhB is mainly due to photobleaching by the excitation light. Here irradiation with UV light was not required, as our dye concentration of 1µM was chosen in such a way as to ensure that due to the thermal equilibrium between on- and off-molecules a sufficient number of molecules was switched on at a given time. Excitation with

#104042 - $15.00 USD Received 12 Nov 2008; revised 3 Dec 2008; accepted 3 Dec 2008; published 4 Dec 2008

circularly polarized light at a wavelength of 532nm allowed us to record two channel images of single isolated pcRhB molecules with a frame rate of 500Hz (Fig. 3(a,b)). We applied circularly polarized light to excite and probe the position and orientation of all fluorophores (and not only of those aligned as parallel as possible to the excitation's polarization direction when applying linearly polarized excitation light). The static behavior of pcRhB in PMMA and its rotational freedom in mowiol is revealed in the two-dimensional anisotropy histograms recorded from a multitude of single pcRhB molecules (Fig. 3(c,d)). In our analysis, we applied a threshold of $n_1 = n_2 = 252$ photons to ensure proper identification of single-molecule fluorescence spots against background, causing the 'black box' of missing events at the origin of the histograms. As expected from theory (compare Fig. 2), static emitters result in a histogram that is predominantly aligned along the two axes (Fig. 3(c)), whereas mobile molecules bear a homogeneous, centrally aligned distribution (Fig. 3(d)). Unlike in theory, the static histogram drops to zero for very low count values n_1 or n_2 in either of the channels. This can be attributed to focusing effects which were neglected in our theoretical analysis and to residual detection noise. Even if the molecule is perfectly aligned with one of the detected polarization channels, this results in photons 'leaking' into the other channel, and thus setting a lower limit to the fraction of photons detected in it. Likewise the freely rotating markers produce a slightly broader histogram than predicted. This can be due to detection noise and possible due to diffusion times which are not considerably faster than the on-times or camera integration times of about 2ms.

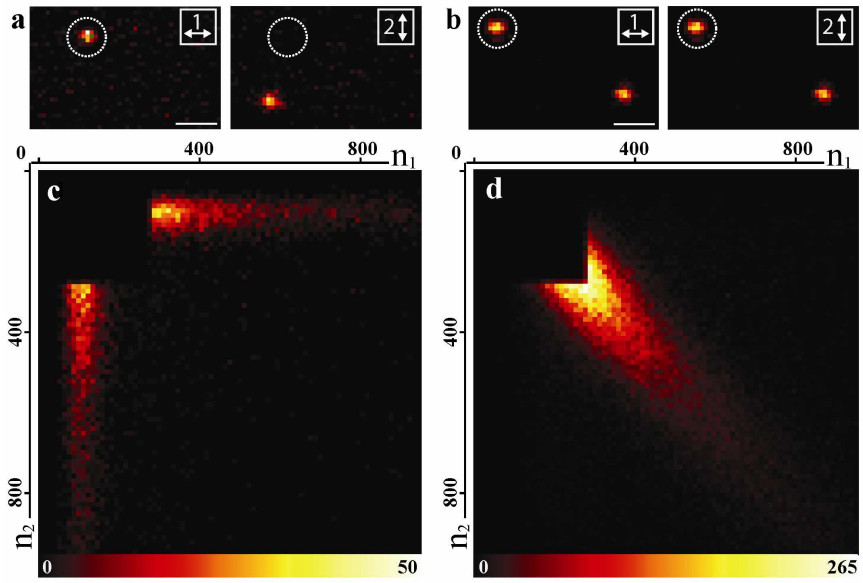

Fig. 3. Two channel images of single pcRhB molecules in (a) PMMA and (b) mowiol. (c) The two-dimensional anisotropy histogram from 9,185 single molecules reveals that pcRhB is static in PMMA. (d) Contrary the histogram from 50,611 pcRhB molecules in mowiol shows that the labels are rotating faster than the event duration. The molecules where excited at 532nm with an intensity of 24 kW/cm^2. Photon threshold $n_1 = n_2 = 252$. Scale bar 1µm.

In order to exemplify how these two-dimensional anisotropy histograms can be used to distinguish between species of different mobility in single-molecule switching based nanoscopy, we prepared a sample comprising of pcRhB labeled silica beads surrounded by the same label in mowiol. Again, we applied a rather large dye concentration and thus the thermal equilibrium between pcRhB molecules in their on- and off-state rendered the use of UV light obsolete. Images recorded at a frame rate of 500 Hz with continuous wave excitation (532nm, 24 kW/cm^2) featured in each frame single isolated fluorescence spots, revealing the position of the respective emitters. Plotting the position of all subsequently recorded molecules

#104042 - $15.00 USD Received 12 Nov 2008; revised 3 Dec 2008; accepted 3 Dec 2008; published 4 Dec 2008

resulted in the image shown in Fig. 4(a). The resolution of the image is limited by the average localization precision which is given by $\Delta r \cong \Delta / \sqrt{<n>/2}$, where Δ is the full-width-half-maximum of the diffraction-limited spot on the camera and $<n>$ is the average number of photons detected per recorded event. The reduction of the localization precision by a factor of two is due to the excess noise introduced by the EMCCD camera at high gain factors [17,23]. Here, we recorded an average of $<n> = 760$ photons for events above threshold resulting in $\Delta r < 14$nm. In practice this higher resolution limit is usually not reached due to limited stability of the setup and inhomogeneous detection background which mostly stems from out-of-focus fluorescence. However, our images clearly exhibit a dramatic resolution gain over the conventional epifluorescent image with its diffraction-limited resolution of about $\Delta = 280$nm (inset Fig. 4(a)). Due to the improved spatial resolution it becomes evident that image quality is compromised because the image is swamped by the homogeneously and densely distributed pcRhB molecules in mowiol. This may be interpreted as a model system for labeled structures in a biological sample with more mobile, excess label in the intracellular fluid. Because we detected multiple photons for each event in the two polarization channels, our method allows us to distinguish between the unwanted background and the bound marker molecules: The position of a label's photon pair (n_1, n_2) in the two-dimensional anisotropy histogram (Fig. 4(b)) allows its assignment to one of the two environments since it can be expected to be static in the beads and freely rotating in mowiol (compare Fig. 3(c,d)). Plotting only those single-molecule events featuring a polarization of $P_n < -0.55$ and $P_n > 0.55$ (Eq. 3), i.e., pair values (n_1, n_2) aligned along the axes of the histogram (Fig. 4(d), green), produces a super-resolved image of just the beads (Fig. 4(c), green) . In contrast, the image of events with a polarization of $-0.15 < P_n < 0.15$, i.e., pair values (n_1, n_2) aligned along the central part of the histogram (Fig. 4(d), red) depicts the homogeneous distribution of pcRhB molecules in mowiol (Fig. 4(c), red).

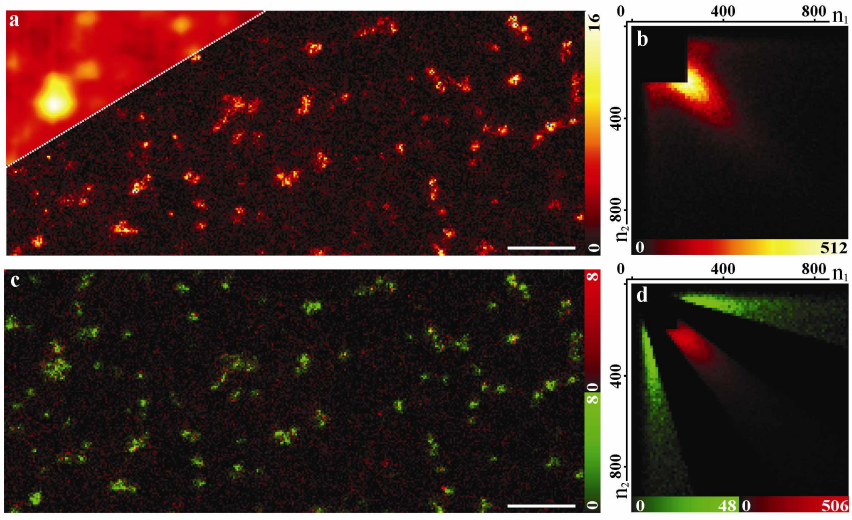

Fig. 4. (a) Nanoscale imaging of pcRhB-labeled beads covered by homogeneously pcRhB-stained mowiol. The upper left corner exemplifies the resolution that a conventional diffraction- limited image would achieve. It was created by adding up the fluorescence detected for all single-molecule events. (b) Two-dimensional anisotropy histogram revealing a distribution with contributions from static pcRhB in beads and rotating dyes in mowiol. (c) By assigning events to two channels based on their position in the histogram, the two species can be spatially separated. Events caused by static molecules are displayed in green and events caused by freely rotating molecules are displayed in red. (d) Histogram of the events shown in (c). Imaging parameters: Excitation at 532nm with 24 kW/cm^2, T = 2 ms, number of frames 30,000, photon threshold $n_1 = n_2 = 252$. Scale bars 1µm.

#104042 - $15.00 USD Received 12 Nov 2008; revised 3 Dec 2008; accepted 3 Dec 2008; published 4 Dec 2008

Importantly, this approach is readily applied to the visualization of rotational mobility of molecules in living cells with nanoscale resolution. Figure 5(a) depicts a nanoscopy image of the ER of a living PtK2 cell. The ER has been labeled with the photoswitchable fluorescent protein rsCherryRev, which switches to its dark state upon excitation with 560nm light and can be switched back on with blue light [30]. The sample was simultaneously irradiated with 560nm light at 16 kW/cm^2 and with 405nm light of an intensity continuously raised from 1 to 10W/cm^2. Raising the 405nm light intensity corrected for the unavoidable decrease of the accessible rsCherryRev concentration due to bleaching and ensured on-off switching of significantly enough single isolated proteins at an almost constant rate. The final nanoscopy image consists of the positions of rsCherryRev molecules gathered over 10,000 frames at a frame rate of 500Hz and an average number of detected photons per event above threshold of $\langle n \rangle$ = 704 ensured a resolution far above that of the conventional image. According to the two-dimensional anisotropy histogram (Fig. 5(b)), all fluorescent proteins observed exhibit a high mobility without an indication for a fraction of static or almost static emitters. This indicates that the proteins move freely within the ER.

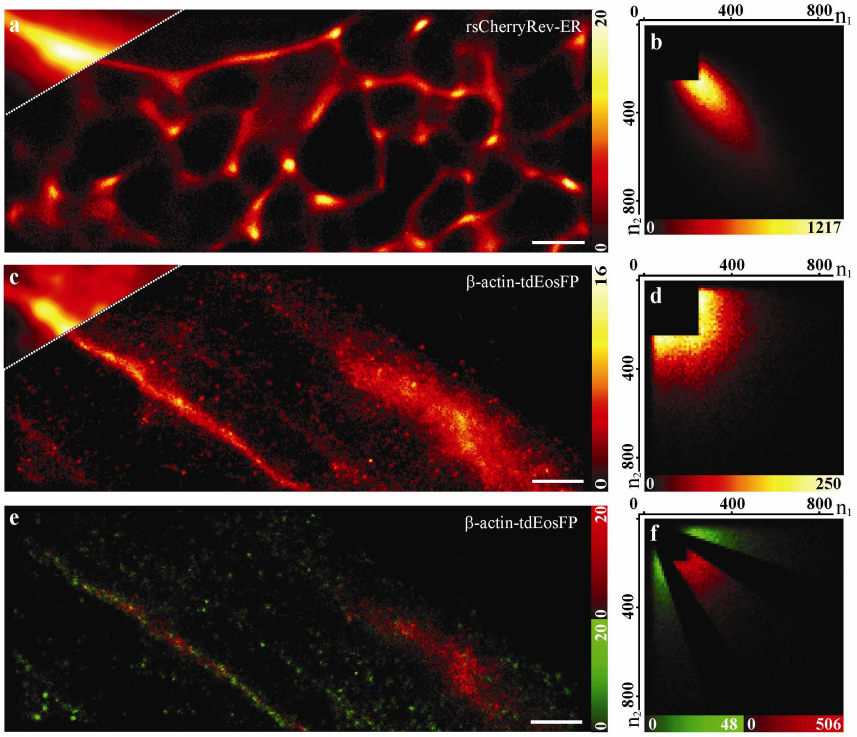

Fig. 5. Nanoscale image of the endoplasmic reticulum (ER) of living PtK2 cells labeled with rsCherryRev (a) and the corresponding two-dimensional anisotropy histogram (b) revealing only mobile rsCherryRev proteins, and of ß-actin of living PtK2 cells labeled with tdEosFP (c). The two-dimensional anisotropy histogram of ß-actin-tdEosFP reveals static and free rotating molecules (d). Separate nanoscopy images of immobile (green) and mobile ß-actin-tdEosFP (red) are created by proper assignment of events based on their position in the two-dimensional anisotropy histogram (f). The resolution of a conventional diffraction-limited image is exemplified in the upper triangles of (a) and (c) where the fluorescence detected for all single-molecule events has been added up. Excitation at 560nm with 16 kW/cm^2 (a) and 8 kW/cm^2 (c), T = 2 ms, number of frames 10,000 and 20,000, photon threshold $n_1 = n_2 = 252$. Scale bars 1µm.

Figure 5(c) shows the nanoscopy image of β-actin in live PtK2 cells labeled with the fluorescent protein tdEosFP. Upon irradiation with 405nm light, EosFP changes the maximum of its absorption from ~505nm to ~570nm and the maximum of its emission from ~515nm to

#104042 - $15.00 USD Received 12 Nov 2008; revised 3 Dec 2008; accepted 3 Dec 2008; published 4 Dec 2008

~580nm [31]. By exciting at 560nm and detecting at > 580nm, we only monitored the fluorescence of tdEosFP switched to its red fluorescent state. The nanoscopy image was recorded for 20,000 frames at a frame rate of 500Hz, with an excitation intensity of 8 kW/cm^2. Again the intensity of the 405nm switch-on light was continuously raised from 1 to 10W/cm^2 in order to correct for the decrease of the accessible proteins due to irreversible photobleaching. The average number of photons per detected event was $\langle n \rangle$ = 680. In contrast to the case of rsCherryRev labeled ER, the two-dimensional anisotropy histogram now reveals a rather inhomogeneous distribution of the molecules' mobility indicating the presence of both, rather static ($P_n < -0.45$ and $P_n > 0.45$) and rather mobile β-actin-tdEosFP ($-0.2 < P_n < 0.2$) molecules (Fig. 5(d)). By using the position of each event in the two-dimensional anisotropy histogram to assign it to one of the two classes (Fig. 5(f)) and plotting them in different colors, the distribution and co-localization of the immobile and mobile molecules is laid out with nanoscale resolution (Fig. 5(e)). Immobile proteins were found to be mainly located at sparsely labeled, probably single actin filaments and broader filament bundles. Furthermore, a part of the immobile β-actin-tdEosFP was located in isolated spots – presumably formed by unspecific aggregation. In contrast, the majority of mobile molecules was found in an unstructured pool within the cytoplasm. A smaller fraction of the mobile fusion proteins was located at actin filament bundles, where they probably take part in building up new fibers suggesting that these mobile proteins are recruited to the filament, but were not yet incorporated into it. Additional β-actin-tdEosFP which may be moving freely within the cytoplasm probably remains undetected in our imaging approach. These molecules with a molecular mass of ~70kDa presumably move through a diffraction-limited area faster than the camera frame time [35]. Therefore photon bursts send out by such molecules will be spread out over a larger area on the camera resulting in a lower probability for such events to generate pixel counts above our detection threshold.

To confirm our findings, we studied the effect of depolymerization of the actin cytoskeleton on the mobility of ß-actin-tdEosFP. To this end, we subjected living PtK2 cells to latrunculin B containing growth medium. Latrunculin B stabilizes monomeric actin – thereby preventing the incorporation of these monomers into fibers. Since the length and the structure of actin filaments is maintained by constant de- and repolymerization – so called tread milling [36] – this stabilization of actin monomers leads to complete depolymerization of the actin network. We recorded three sets of nanoscopy images: (i) before incubation, (ii) 15-25 min after incubation with latrunculin B and (iii) another 30 min after replacing the toxin containing medium with normal culture medium. The average anisotropy histograms of all events recorded from three PtK2 cells respectively are depicted in Fig. 6. Upon incubation with latrunculin B, the mobile fraction of β-actin-tdEosFP clearly increases (Fig. 6(a,b)). At the same time the actin cytoskeleton disintegrates as witnessed in the wide-field images shown in the inset. After replacing the latrunculin B containing medium by drug-free growth medium, the static fraction increased again (Fig. 6(c)). This indication that the actin filaments have re-formed is also consistent with the corresponding wide-field image.

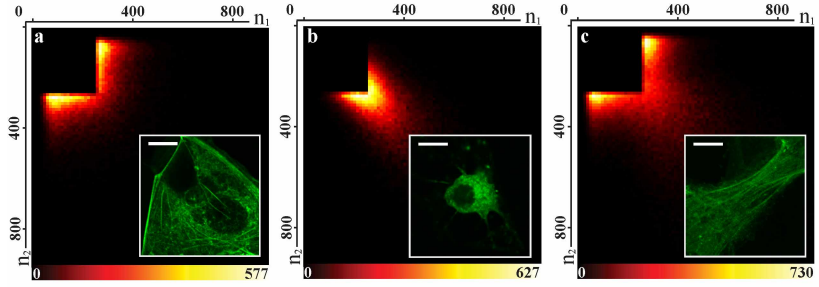

Fig. 6. Two-dimensional anisotropy histograms of live PtK2 cells expressing ß-actin-tdEosFP (a) in a normal culture medium, (b) after 15-25 minutes of incubations with latrunculin B and (c) after 30 minutes of recovery from the toxin. All histograms show events from three cells. The insets show wide-field images of exemplary cells. Photon threshold $n_1 = n_2 = 252$. Scale bars 10µm.

#104042 - $15.00 USD Received 12 Nov 2008; revised 3 Dec 2008; accepted 3 Dec 2008; published 4 Dec 2008

5. Conclusion

In this study we have for the first time combined optical nanoscopy and polarization sensitive detection. Because our experimental approach is single-molecule based, we can measure probability distributions of characteristic count pairs by plotting two-dimensional frequency histograms of the photon pairs detected from a multitude of molecules. These histograms can be used to distinguish between molecular species of different rotational mobility, which is a major advantage over ensemble measurements where at best a single anisotropy value can be extracted per sample region. We have demonstrated how this method can be used for the separation of ß-actin already incorporated in filaments and freely rotating molecules in nanoscopic images of living PtK2 cells.

Importantly, our concept lends itself directly to a wide range of applications like probing of the physical microenvironment of bound or slowly diffusing unbound molecules through determination of their rotational diffusion speed, or distinguishing several binding sites targeted by the same label. The time scale of the present approach is given by the time a single label needs to emit enough detectable photons in order to be localized with nanoscale precision. When using a targeted (focal spot based) read-out mode as in STED microscopy, the position does not depend on the number of detected photons, because the position is already known and m molecules can be detected at the same time. However, contrary to the approach presented herein, the information is not on the single molecule level, unless there is just a single molecule m=1 in the spot.

In our experiments we have used circularly polarized light to both switch and excite the markers. Using linearly polarized excitation and/or activation light will render the data analysis more complex but yields additional information about the mobility of the markers. For example, linearly polarized excitation can be used to combine our method with traditional anisotropy measurements on individual markers thus measuring their rotational diffusion on a wider range of time scales.

The exploitation of the fluorescence polarization to realize functional nanoscopy is in line with a previous approach based on spectral separation [22,23]. Our present choice of polarization-sensitive detection is readily combined with the spectrally-sensitive detection to further optimize molecular recognition and characterization. Several other parameters of fluorescence emission are already routinely probed in single-molecule spectroscopy and we expect them to be exploited in a similar fashion in the near future. Determination of the fluorescence lifetime [37] or the efficiency of Förster resonance energy transfer (FRET) [21] at the single molecule level will be important steps towards an almost complete, spatially resolved molecular characterization of biological samples. It is also important to note that the choice of labels is not limited to special photoswitchable, say activatable, fluorophores. Conventional organic dyes or fluorescent proteins lend themselves to the same concept and may provide more optimal labeling [38]. Finally, markers which are read out by signals other than fluorescence or switched through other mechanisms than absorption of light are also conceivable. The only necessary ingredient are two states with a controllable transition probability where the switching process results in a notable change of a read-out signal measurable in the far-field [4,5]. Such new constructs may feature other parameters that can then be probed on a single-emitter level and carry additional information about the sample. Combining spectroscopy and nanoscopy in the way outlined in this manuscript will open a whole new field of applications in the life sciences and beyond.

Acknowledgments

We thank Tanja Gilat and Rita Schmitz-Salue for excellent technical assistance. We acknowledge Vladimir Belov for supplying pcRhB. We also acknowledge Rainer Pick for help with the technical design of the setup and thank J. Jethwa for critical reading the manuscript.

#104042 - $15.00 USD Received 12 Nov 2008; revised 3 Dec 2008; accepted 3 Dec 2008; published 4 Dec 2008